International Journal of Chemical Kinetics

WILEY

RESEARCH ARTICLE OPEN ACCESS

Rate Coefficients for the Cl Atom Gas-Phase Reaction With Permethylsiloxanes (PMS): L_2, L_3, L_4, L_5, D_3, D_4, D_5, and D_6

Daniel Van Hoomissen[1,2] | Aparajeo Chattopadhyay[1,2] | James B. Burkholder[1]

[1]Chemical Sciences Laboratory, National Oceanic and Atmospheric Administration, Boulder, Colorado, USA | [2]Cooperative Institute for Research in Environmental Sciences, University of Colorado, Boulder, Colorado, USA

Correspondence: James B. Burkholder (James.B.Burkholder@noaa.gov)

Received: 23 August 2024 | **Revised:** 22 October 2024 | **Accepted:** 20 November 2024

Funding: The authors received no specific funding for this work.

Keywords: Cl atom | gas-phase reaction | permethylsiloxanes | rate coefficients

ABSTRACT

Rate coefficients, k(T), for the gas-phase Cl atom reaction with hexamethyldisiloxane ($(CH_3)_3SiOSi(CH_3)_3$, L_2), k_1; octamethyltrisiloxane ($[(CH_3)_3SiO]_2Si(CH_3)_2$, L_3), k_2; decamethyltetrasiloxane ($(CH_3)_3SiO[Si(CH_3)_2O]_2Si(CH_3)_3$, L_4, k_3; dodecamethylpentasiloxane ($(CH_3)_3SiO[Si(CH_3)_2O]_3Si(CH_3)_3$, L_5, k_4; hexamethylcyclotrisiloxane ($[\text{-}Si(CH_3)_2O\text{-}]_3$, D_3), k_5; octamethylcyclotetrasiloxane ($[\text{-}Si(CH_3)_2O\text{-}]_4$, D_4), k_6; decamethylcyclopentasiloxane ($[\text{-}Si(CH_3)_2O\text{-}]_5$, D_5, k_7), and dodecamethylcyclohexasiloxane ($[\text{-}Si(CH_3)_2O\text{-}]_6$, D_6, k_8) were measured over a range of temperature (273–363 K) using a pulsed laser photolysis (PLP) – resonance fluorescence (RF) technique. The obtained k(296 K) and Arrhenius expressions with 2σ uncertainties including estimated systematic errors are (in units of 10^{-10} cm^3 molecule^{-1} s^{-1}):

L_2: k_1(296 K) = (1.58 ± 0.07)	k_1(273–363 K) = (1.36 ± 0.10) exp((43 ± 249)/T)
L_3: k_2(296 K) = (1.93 ± 0.09)	k_2(273–353 K) = (1.95 ± 0.18) exp((1 ± 632)/T)
L_4: k_3(296 K) = (2.36 ± 0.12)	k_3(273–353 K) = (2.09 ± 0.16) exp((43± 522)/T)
L_5: k_4(296 K) = (2.84 ± 0.19)	k_4(296–353 K) = (2.70 ± 0.18) exp((15 ± 490)/T)
D_3: k_5(296 K) = (0.588 ± 0.028)	k_5(273–353 K) = (0.47 ± 0.03) exp((78 ± 470)/T)
D_4: k_6(296 K) = (1.13 ± 0.06)	k_6(273–353 K) = (1.14 ± 0.07) exp((4 ± 432)/T)
D_5: k_7(296 K) = (1.72 ± 0.09)	k_7(273–353 K) = (1.60 ± 0.10) exp((22 ± 432)/T)
D_6: k_8(296 K) = (2.16 ± 0.14)	k_8(296–353 K) = (1.73 ± 0.14) exp((71 ± 562)/T)

The cyclic permethyl siloxanes (cyclic PMS) were found to be less reactive than the analogous linear permethyl siloxane (linear PMS) with an equal number of CH_3- groups. Both linear and cyclic compounds show a linear relationship between the measured rate coefficient and the number of CH_3- groups in the molecule. A structure–activity relationship (SAR) is presented that reproduces the experimental data to within ~10% at all temperatures. For [Cl] ≈ 10^4 atom cm^{-3}, an approximate free troposphere abundance, the PMS loss due to Cl atom reaction leads to relatively short estimated lifetimes of 7, 6, 5, 4, 20, 10, 7, and 5 days for L_2, L_3, L_4, L_5, D_3, D_4, D_5, and D_6, respectively. Therefore, the PMSs included in this study are classified as atmospherically very short-lived substances and Cl atom reaction represents a significant loss process.

1 | Introduction

Permethylsiloxanes (PMSs) are a class of volatile organic compounds present in many household, cosmetic, and industrial products [1, 2]. Linear and cyclic forms of PMS have been measured in a variety of environments including indoor [3], urban [4], rural [5], and global regions [1, 6, 7]. Abundant PMSs, namely dodecamethylpentasiloxane (D_5), are currently being used as tropospheric gas-phase tracers of human activity, in part, due to their prevalence in cosmetic products [2, 4, 8]. As a result of the relatively poor water solubility and high vapor pressures of PMSs, especially for the lower molecular weight (MW) compounds, PMSs will readily partition into the gas phase [6]. An understanding of the oxidation of atmospherically relevant PMS is crucial to elucidating their environmental fate. In the gas phase, the predominant atmospheric loss of PMSs is expected to be by reaction with the OH radical [9–16] and Cl atom [14, 17–19]. Recent studies from this laboratory have reported temperature-dependent reaction rate coefficients, k(T), for four cyclic (D_3, D_4, D_5, and D_6) and linear (L_2, L_3, L_4, and L_5) PMSs [15, 20]. The Cl atom kinetics of PMS are thought to proceed through methyl group H-atom abstraction analogous to OH kinetics. Therefore, the atmospheric degradation of PMSs initiated by the OH radical or Cl atom is expected to lead to the same oxidation products, for example, siloxanol, siloxane formate esters, and other oxygenated products [21], that can contribute to secondary aerosol formation (SOA) [22–28].

There have been several studies of Cl + PMS reactions available in the literature that applied relative rate kinetic methods to determine room temperature rate coefficients [14, 17, 19]. Most recently, rate coefficients were determined for a series of linear (L_2, L_3, L_4, and L_5) and cyclic (D_3, D_4, D_5, and D_6) PMS from chamber studies using time-of-flight (ToF) chemical ionization (CI) [17], all compounds except D_6, and proton transfer (PTR) [19] mass spectrometry detection methods. Reaction rate coefficients were reported to be in the range $(0.5–2.7) \times 10^{-10}$ cm^3 molecule^{-1} s^{-1} with rate coefficients increasing with increasing number of methyl groups, while cyclic PMSs were found to be less reactive than the analogous linear PMS with an equivalent number of methyl groups. This is a reactivity trend similar to that observed for the OH radical reaction [15, 20]. The absolute 1σ uncertainties in the literature Cl atom reaction rate coefficients were quoted to be as high as 30%. Prosmitis et al. [18] studied the Cl + L_2 reaction over the temperature range 273–363 K at low pressure, which is the only available temperature-dependent study. They reported a weak rate coefficient temperature dependence with $E/R = 11 \pm 136$ K. The large uncertainty in the Cl + PMS reported rate coefficients combined with a lack of comprehensive temperature-dependent rate coefficients for atmospherically relevant PMS warrants further study to evaluate the reactivity and impact of PMSs on the environment.

In this study, the rate coefficients for the Cl atom gas-phase reaction with the four simplest linear and cyclic PMSs were measured over a range of temperatures using the pulsed laser photolysis (PLP) – resonance fluorescence (RF) absolute kinetic method:

$$Cl + L_2 \rightarrow \text{products}\,(k_1) \quad (1)$$

$$Cl + L_3 \rightarrow \text{products}\,(k_2) \quad (2)$$

$$Cl + L_4 \rightarrow \text{products}\,(k_3) \quad (3)$$

$$Cl + L_5 \rightarrow \text{products}\,(k_4) \quad (4)$$

$$Cl + D_3 \rightarrow \text{products}\,(k_5) \quad (5)$$

$$Cl + D_4 \rightarrow \text{products}\,(k_6) \quad (6)$$

$$Cl + D_5 \rightarrow \text{products}\,(k_7) \quad (7)$$

$$Cl + D_6 \rightarrow \text{products}\,(k_8) \quad (8)$$

Figure S1 shows the structures of the linear and cyclic PMSs studied in this work: hexamethyldisiloxane (L_2), octamethyltrisiloxane (L_3), decamethyltetrasiloxane (L_4), dodecamethylpentasiloxane (L_5), hexamethylcyclotrisiloxane (D_3), octamethylcyclotetrasiloxane (D_4), decamethylcyclopentasiloxane (D_5), and dodecamethylcyclohexasiloxane (D_6).

2 | Experimental Details

Rate coefficients, k(T), for Reactions (1)–(8) were measured at temperatures between 273 and 353 K at total pressures between 50 and 250 Torr (He bath gas) using a PLP – RF technique. Due to limitations of the L_5 and D_6 vapor pressure, rate coefficient measurements were only performed over a slightly more limited temperature range, 296–353 K. The PLP-RF apparatus has been used previously in our laboratory and is described in detail elsewhere [29–31]. The jacketed Pyrex RF reactor had an internal volume of ~250 cm^3 and multiple orthogonal ports for the Cl atom resonance lamp, PLP beam, and the solar blind PMT detector. The reactor was temperature-regulated (±1 K) by circulating fluid from a temperature-regulated reservoir through the reactor jacket. Kinetic measurements were performed under slow gas-flow conditions.

Cl atoms were produced by pulsed excimer laser photolysis of chlorine, Cl_2, at 308 nm (XeCl laser) and 351 nm (XeF laser):

$$Cl_2 + h\nu \rightarrow 2Cl \quad (9)$$

where the quantum yield for Cl atom production is 2, or by the photolysis of oxalyl chloride, $(COCl)_2$, at 308 nm:

$$(COCl)_2 + h\nu \rightarrow 2Cl + 2CO \quad (10a)$$

$$\rightarrow Cl + ClCO + CO \quad (10b)$$

The Cl atom quantum yield in Reaction (10) at 308 nm has not been reported in the literature, but previous $(COCl)_2$ photolysis work in our laboratory using 248 and 351 nm photolysis would imply a Cl quantum yield greater than ~1.5 at the pressures used in the present study [32]. We assume a conservative upper-limit quantum yield of 2 for estimating Cl atom production. ClCO produced in channel 10b will decompose to Cl + CO at

the pressures of the present experiments within 100 μs following the photolysis laser pulse [33]. Therefore, there is a prompt Cl atom production combined with a smaller rapid secondary formation, which does not interfere with the kinetic analysis of Reactions (1)–(8).

The photolysis laser beam passed through a 0.65 cm^2 aperture and the laser power was measured at the exit of the reactor after passing through two quartz windows. The photolysis laser fluence, F, was varied over the course of the study over the 4.8–32 mJ cm^{-2} $pulse^{-1}$ range for 308 nm photolysis and 2.1–15 mJ cm^{-2} $pulse^{-1}$ for 351 nm photolysis. The initial Cl atom concentration, $[Cl]_0$, was estimated to be in the range (1.2–20) × 10^{11} atom cm^{-3}, over the course of this study, based on the photolysis laser fluence, precursor concentration, and absorption cross section at the photolysis wavelength, $\sigma(\lambda)$, and precursor quantum yield, $\Phi(\lambda)$:

$$[Cl]_0 = \sigma(\lambda) \times \phi(\lambda) \times [\text{Precursor}] \times F \quad \text{(I)}$$

Absorption cross sections were taken from Burkholder et al. [34].

Cl atoms were detected via VUV fluorescence from the $^{2,4}P_{1/2} \leftarrow {}^2P_{3/2}$ Cl atomic transitions at 134.73 and 136.35 nm [35]. The 20 W microwave resonance lamp was equipped with a CaF_2 window and was operated with a slow flow of a 3% Cl_2 in He mixture further diluted with an additional He flow (effective ~0.4% Cl_2 in He mixture in the lamp) at a total pressure of ~2.8 Torr. Fluorescence was collected via a 15 cm focal length MgF_2 lens mounted in front of the solar-blind photomultiplier tube that was orthogonal to the resonance lamp and the photolysis laser beam. The PMT signal was fed into a 100 MHz amplifier-discriminator and then to a digital counting acquisition board (32-bit, 80 MHz). Temporal profiles were collected in 5 or 10 μs bins. Temporal profiles were typically collected by adding 2000, or more, profile measurements together, that is, photolysis laser pulses. The data acquisition started 1 ms prior to the photolysis laser pulse and profiles were recorded for a total of 10–20 ms. The Cl atom detection limit (S/N = 1) was estimated to be ~5 × 10^8 atom cm^{-3} for 1 s integration with 100 Torr He bath gas.

Rate coefficients were measured under pseudo-first-order conditions in Cl, for example, [PMS] ≫ [Cl]. When $(ClCO)_2$ was used as the Cl atom precursor, Cl atom temporal profiles were described by a first-order rate expression:

$$\ln\left(\frac{[Cl]_t}{[Cl]_0}\right) = \ln\left(\frac{S_t}{S_0}\right) = -(k[\text{PMS}] + k_d)t = k't \quad \text{(II)}$$

where S_t and S_0 are the measured Cl atom signal at time t and 0, when the photolysis laser fires, respectively, and k' and k_d are the first-order rate coefficients for the loss of Cl atoms in the presence and absence of PMS, respectively. k_d is primarily determined by Cl atom flow out of the detection region, but also contains primarily first-order loss processes that are independent of the PMS concentration. k_d values were in the range 18 to 200 s^{-1}. When Cl_2, in the absence of added O_2, was used as the Cl atom source, the Cl atom temporal profiles were described by a double exponential decay:

$$\left(\frac{S_t}{S_0}\right) = A\exp(-k't) + B\exp(-k''t) \quad \text{(III)}$$

where $k' = k_{1\text{-}8}[\text{PMS}] + k_d$ and $k'' = k_{11}[Cl_2]$. k_{11} represents the rate coefficient for the regeneration of Cl atoms in the reaction of Cl_2 with the radical product formed in Reactions (1)–(8), for example:

$$Cl_2 + (CH_3)_3SiOSi(CH_3)_2CH_2 \rightarrow (CH_3)_3SiOSi(CH_3)_2CH_2Cl + Cl \quad (11)$$

In some experiments, O_2 was added to the reaction mixture, (3.5–14.5) × 10^{15} molecule cm^{-3}, to scavenge the siloxane radical formed in Reactions (1)–(8) to form a peroxy radical, for example:

$$(CH_3)_3SiOSi(CH_3)_2CH_2 + O_2 \rightarrow (CH_3)_3SiOSi(CH_3)_2CH_2O_2 \quad (12)$$

eliminating the generation of secondary Cl atoms. The addition of sufficient O_2 resulted in single exponential Cl atom decays that were analyzed using Equation (2). The use of intermediate O_2 concentrations enabled an estimate for the rate coefficient of Reaction (12).

Online UV and infrared absorption, measurements were used to determine the PMS concentration in the RF reactor. The UV absorption measurement was performed before the reactor using an Hg Pen-ray lamp light source equipped with a 185 nm band pass filter, 100 cm long (1.9 cm i.d.) Pyrex absorption cell equipped with quartz windows, and a photodiode at the cell exit coupled with 185 nm band pass filter. A beam splitter mounted before the entrance to the absorption cell coupled a fraction of the light source to an orthogonal photodiode detector and 185 nm bandpass filter to monitor fluctuations in the 185 nm light intensity. The PMS and bath gas flows were mixed and passed through the absorption cell, after which the Cl atom precursor ($(COCl)_2$ or Cl_2) and radical scavenger/quencher (O_2, SF_6) (if present) was introduced to the flow prior to entering the RF reactor. The 185 nm absorption cross sections for L_2, L_3, D_3, and D_4 were measured previously in our laboratory [15]. For L_4, L_5, D_5, and D_6, PMS/He gas mixtures were prepared manometrically off-line in 12 L Pyrex bulbs, and their 185 nm cross sections were determined relative to their infrared cross sections measured previously by Bernard et al. [36]. Absorption cross sections at 185 nm of (10.1 ± 0.6), (12.1 ± 1.7), (6.62 ± 0.7), and (7.72 ± 0.7) (10^{-18} cm^2 $molecule^{-1}$) were obtained for L_4, L_5, D_5, and D_6, respectively, where the uncertainties are 2σ measurement precision.

Infrared absorption spectra were measured online using a Fourier transform infrared spectrometer (FTIR) equipped with a ~500 cm^3 multi-pass absorption cell (485 cm path length, KBr windows). Spectrum measurements were recorded at 296 K between 500 and 4000 cm^{-1} at 1 cm^{-1} resolution. Absorption spectra were recorded after the gases passed through the reactor and were quantified using the PMS spectra determined previously in this laboratory [36]. The PMS concentration determined by the infrared absorption measurements provided the primary determination of PMS concentration in the reactor, following adjustments for differences in temperature and pressure, used in the determination of $k_1(T) - k_8(T)$.

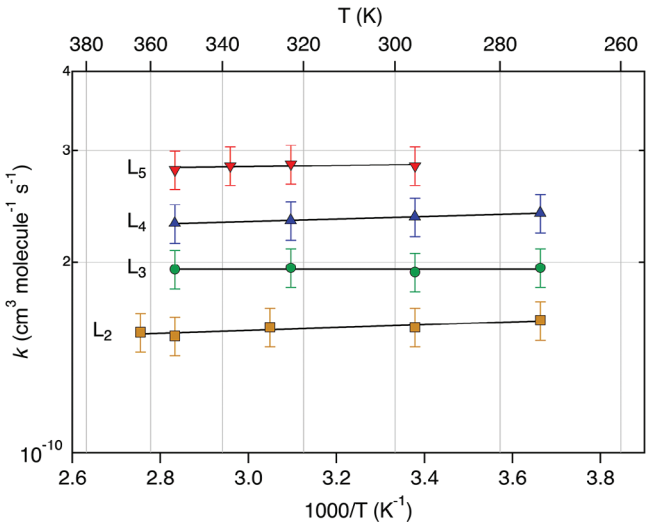

FIGURE 1 | Arrhenius plot for the Cl + linear permethylsiloxanes (PMS) L_2, L_3, L_4, and L_5 rate coefficient data obtained in this work. The lines are least-squares fits of the linearized data (see Tables 1–4). The data error bars correspond to 2σ absolute uncertainty.

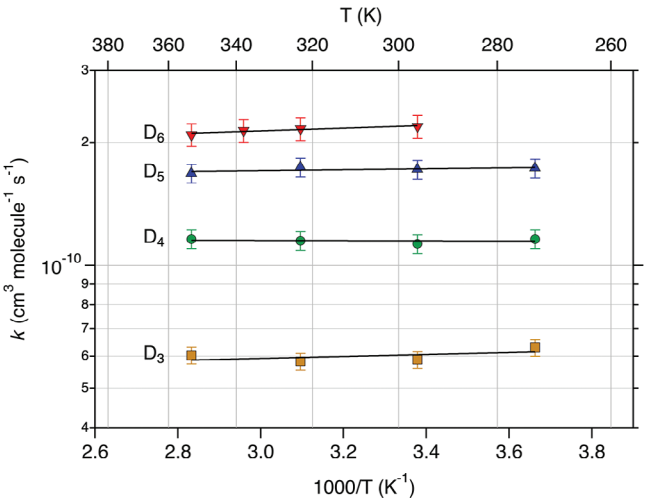

FIGURE 2 | Arrhenius plot for the Cl + linear permethylsiloxanes (PMS) D_3, D_4, D_5, and D_6 rate coefficient data obtained in this work. The lines are least-squares fits of the linearized data (see Tables 5–8). The data error bars correspond to 2σ absolute uncertainty.

3 | Materials

He (UHP, 99.999%), O_2 (UHP, 99.99%), Cl_2 (0.4 and 3% Cl_2/He mixtures, UHP, 99.999%), and SF_6 (99.9%) were used as supplied. $(COCl)_2$ (≥99%) was purified via several freeze (77 K)-pump-thaw cycles. The stated purities of L_2, L_3, D_3, D_4, and D_6 was ≥98%. The reported purity of the L_4, L_5, and D_5 samples was ≥97%. The PMS samples were degassed in several freeze (77 K)-pump-thaw cycles and stored under vacuum in Pyrex reservoirs. The L_2, L_3, D_3, and D_4 samples were purified via vacuum distillation to remove cross PMS impurities as described in Bernard et al. [15] $(COCl)_2$ was introduced into the reactor from a manometrically prepared $(COCl)_2$/He mixture with mixing ratios ranging from ~0.5%–2.5%. Cl_2 was introduced into the RF reactor and resonance lamp from a dilute commercial mixture (3% Cl_2 in He). L_2, L_3, D_3, and D_4 were introduced into the flow system from manometrically prepared dilute mixtures in He bath gas; mixing ratios were in the range (1.0–6.0) × 10^{-3}. L_4, L_5, D_5, and D_6 were swept into the gas flow by passing a flow of He carrier gas through a vacuum sample reservoir containing the pure compound. Gas flows were measured using calibrated electronic flow meters and pressures were measured using 100 and 1000 Torr capacitance manometers. Quoted uncertainties are 2σ (95% confidence level) unless stated otherwise.

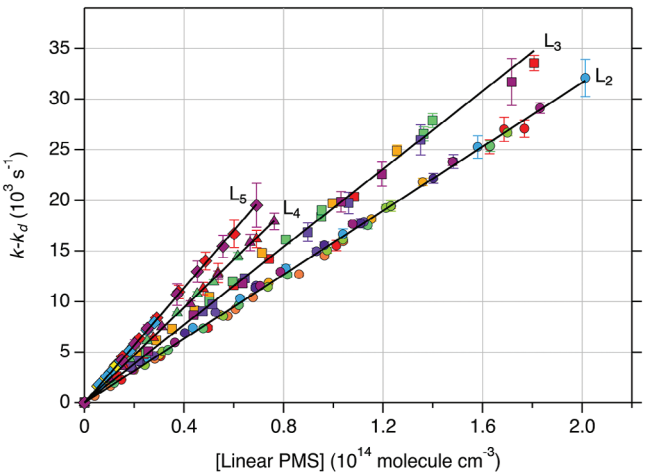

FIGURE 3 | Rate coefficient data (k-k_d) for the Cl atom + linear permethylsiloxane (PMS) reactions measured in this work at 296 K: hexamethyldisiloxane ($(CH_3)_3SiOSi(CH_3)_3$, L_2; octamethyltrisiloxane ($[(CH_3)_3SiO]_2Si(CH_3)_2$, L_3; decamethyltetrasiloxane ($(CH_3)_3SiO[Si(CH_3)_2O]_2Si(CH_3)_3$, L_4; dodecamethylpentasiloxane ($(CH_3)_3SiO[Si(CH_3)_2O]_3Si(CH_3)_3$, L_5) reaction (see Tables 1–4). The lines are linear least-squares fits of the combined datasets. Individual experiments are denoted by different marker colors. The data error bars are 2σ of the linear least-squares fit of the Cl atom decay.

4 | Results and Discussion

4.1 | Rate Coefficient Measurements

k(T) measurements for the Cl + PMS reactions were carried out using the PLP–RF method for temperatures in the range 273 to 353 K at total pressures between 50 and 250 Torr (He bath gas). There was no rate coefficient pressure dependence observed under this range of experimental conditions. A summary of the experimental conditions and the measured rate coefficients for Reactions (1)–(8) are given in Tables 1–8. The rate coefficients for all reactions show a negligible temperature dependence for the range of temperatures included in this study, see Figures 1 and 2. Fits of the data to an Arrhenius expression are given in Table 9.

The measured Cl atom decay profiles obtained using the $(COCl)_2$ and Cl_2 (with O_2 added) were single exponential. Representative decay profiles are given in Figures S2–S9 with measured k' values in the 1260 to 22,300 s^{-1} range for cyclic PMSs and 660 to 33,600 s^{-1} for linear PMSs. Second-order kinetic plots of the room temperature data are shown in Figures 3 and 4. Data obtained at other temperatures was of similar quality. Figures 3 and 4 also

TABLE 1 | Summary of experimental conditions and rate coefficients obtained in this work for the Cl + hexamethyldisiloxane ($(CH_3)_3SiOSi(CH_3)_3$, L_2) reaction.

				Cl atom source parameters					
T (K)	**P (Torr, He)**	**$[O_2]$ (10^{15} molecule cm^{-3})**	**Linear flow velocity (cm s^{-1})**	**Cl atom precursor**	**[Precursor] (10^{14} molecule cm^{-3})**	**Photolysis laser fluence (mJ cm^{-2} $pulse^{-1}$)**	**$[Cl]_0$ (10^{11} molecule cm^{-3})**	**$[L_2]$ Range (10^{14} molecule cm^{-3})**	**k(T)[a] (10^{-10} cm^3 $molecule^{-1}$ s^{-1})**
273	100	9.4	4.7	Cl_2	1.92	4.0	5.2	0.09–1.91	1.62 ± 0.03
296	100	3.5	14.1	Cl_2	0.78	2.1	1.2	0.13–1.77	1.56 ± 0.03
296	100	7.5	14.1	Cl_2	0.91	7.7	4.8	0.04–1.01	1.51 ± 0.02
296	200	8.7	6.2	Cl_2	2.07	7.2	10	0.20–1.35	1.59 ± 0.01
296	50	7.9	12.7	Cl_2	0.96	7.8	5.1	0.24–1.65	1.57 ± 0.01
296	100	9.1	5.4	Cl_2	2.23	5.3	8.0	0.20–1.14	1.55 ± 0.01
296	125	-	7.5	$(COCl)_2$	0.97	23	5.7	0.25–2.01	1.61 ± 0.02
296	150	-	6.2	$(COCl)_2$	0.95	23	5.6	0.26–1.45	1.62 ± 0.03
296	100	-	8.9	$(COCl)_2$[c]	2.29	11	6.2	0.21–1.32	1.61 ± 0.03
296	150	-	6.8	$(COCl)_2$[d]	2.59	17	11	0.20–1.84	1.61 ± 0.02
								Global Fit[b]	1.58 ± 0.01
328	100	9.0	4.9	Cl_2	1.65	4.4	4.9	0.24–1.96	1.58 ± 0.02
328	100	6.0	5.6	Cl_2	1.93	4.0	5.3	0.35–1.39	1.57 ± 0.02
								Global Fit[b]	1.58 ± 0.02
353	100	7.7	6.4	Cl_2	1.87	5.1	6.4	0.39–1.47	1.53 ± 0.01
363	100	7.3	12.3	Cl_2	1.16	15	12	0.07–1.18	1.55 ± 0.02

[a]Quoted uncertainties are 2σ precision of the non-weighted linear least-squares fits with the intercept set to the background loss rate coefficient (k_d).

[b]Global linear least-squares fits (2σ precision) of the combined k(T)-k_d dataset with the intercept fixed to the origin.

[c]Sulfur hexafluoride (SF_6) concentration of 3.7×10^{16} molecule cm^{-3} added to the reaction mixture.

[d]Sulfur hexafluoride (SF_6) concentration of 1.2×10^{16} molecule cm^{-3} added to the reaction mixture.

TABLE 2 | Summary of experimental conditions and rate coefficients obtained in this work for the Cl + octamethyltrisiloxane ($[(CH_3)_3SiO]_2Si(CH_3)_2$, L_3) reaction.

				Cl atom source parameters					
T (K)	**P (Torr, He)**	**$[O_2]_0$ (10^{15} molecule cm^{-3})**	**Linear flow velocity (cm s^{-1})**	**Cl atom precursor**	**[Precursor] (10^{14} molecule cm^{-3})**	**Photolysis laser fluence (mJ cm^{-2} pulse^{-1})**	**$[Cl]_0$ (10^{11} molecule cm^{-3})**	**$[L_3]$ Range (10^{14} molecule cm^{-3})**	**k(T)[a] (10^{-10} cm^3 molecule^{-1} s^{-1})**
273	100	7.7	5.7	Cl_2	1.22	10	12	0.32–1.43	1.94 ± 0.02
273	100	6.5	5.3	Cl_2	1.21	9.7	8.0	0.26–1.37	2.00 ± 0.03
								Global Fit[b]	1.96 ± 0.02
296	150	-	5.6	$(COCl)_2$	0.83	31	6.3	0.13–1.08	1.88 ± 0.03
296	150	6.2	5.5	$(COCl)_2$	1.68	31	13	0.22–1.02	2.01 ± 0.03
296	99	8.0	4.5	Cl_2	1.48	9.9	9.6	0.25–1.40	1.98 ± 0.02
296	50	6.8	6.7	Cl_2	1.61	11	12	0.19–1.35	1.90 ± 0.02
296	100	9.4	3.6	Cl_2	2.77	3.9	7.4	0.26–1.72	1.88 ± 0.03
								Global Fit[b]	1.93 ± 0.02
323	100	6.3	5.5	Cl_2	1.09	9.6	7.1	0.20–1.06	1.96 ± 0.02
353	50	6.3	7.8	Cl_2	0.77	13	5.1	0.11–1.23	1.95 ± 0.04
353	100	7.2	5.3	Cl_2	1.24	10	8.5	0.27–1.13	1.95 ± 0.02
								Global Fit[b]	1.95 ± 0.02

[a]Quoted uncertainties are 2σ precision of the non-weighted linear least-squares fits with the intercept set to the background loss rate coefficient (k_d).
[b]Global linear least-squares fits (2σ precision) of the combined k(T)-k_d dataset with the intercept fixed to the origin.

TABLE 3 | Summary of experimental conditions and rate coefficients obtained in this work for the Cl + decamethyltetrasiloxane ($(CH_3)_3SiO[Si(CH_3)_2O]_2Si(CH_3)_3$, L_4) reaction.

			Cl atom source parameters					
T (K)	P (Torr, He)	Linear flow velocity (cm s^{-1})	Cl atom precursor	[Precursor] (10^{14} molecule cm^{-3})	Photolysis laser fluence (mJ cm^{-2} $pulse^{-1}$)	$[Cl]_0$ (10^{11} molecule cm^{-3})	$[L_4]$ Range (10^{14} molecule cm^{-3})	k(T)[a] (10^{-10} cm^3 $molecule^{-1}$ s^{-1})
273	200	8.3	$(COCl)_2$	2.00	14	6.9	0.18–0.84	2.37 ± 0.05
273	250	9.0	$(COCl)_2$	2.76	11	7.4	0.15–0.77	2.40 ± 0.02
							Global Fit[b]	2.39 ± 0.03
296	150	10.3	$(COCl)_2$	3.09	12	9.2	0.16–0.69	2.36 ± 0.02
296	125	12.7	$(COCl)_2$	1.67	22	9.0	0.09–0.62	2.35 ± 0.03
296	125	14.9	$(COCl)_2$	1.76	12	5.4	0.10–0.76	2.36 ± 0.02
							Global Fit[b]	2.36 ± 0.02
323	125	14.0	$(COCl)_2$	1.35	20	6.8	0.15–0.95	2.37 ± 0.03
323	200	12.1	$(COCl)_2$	1.19	12	3.7	0.15–0.67	2.34 ± 0.02
							Global Fit[b]	2.33 ± 0.02
353	150	14.7	$(COCl)_2$	1.10	19	5.3	0.17–0.72	2.30 ± 0.02
353	200	11.2	$(COCl)_2$	1.40	16	5.4	0.13–0.74	2.31 ± 0.03
							Global Fit[b]	2.30 ± 0.02

[a]Quoted uncertainties are 2σ precision of the non-weighted linear least-squares fits with the intercept set to the background loss rate coefficient (k_d).
[b]Global linear least-squares fits (2σ precision) of the combined k(T)-k_d dataset with the intercept fixed to the origin.

TABLE 4 | Summary of experimental conditions and rate coefficients obtained in this work for the Cl + dodecamethylpentasiloxane ($(CH_3)_3SiO[Si(CH_3)_2O]_3Si(CH_3)_3$, L_5) reaction.

			Cl atom source parameters					
T (K)	P (Torr, He)	Linear flow velocity (cm s^{-1})	Cl atom precursor	[Precursor] (10^{14} molecule cm^{-3})	Photolysis laser fluence (mJ cm^{-2} $pulse^{-1}$)	$[Cl]_0$ (10^{11} molecule cm^{-3})	$[L_5]$ Range (10^{14} molecule cm^{-3})	k(T)[a] (10^{-10} cm^3 $molecule^{-1}$ s^{-1})
296	125	13.1	$(COCl)_2$	1.59	17	10	0.15–0.60	2.85 ± 0.05
296	175	10.4	$(COCl)_2$	2.56	17	11	0.05–0.68	2.87 ± 0.04
296	125	8.4	$(COCl)_2$	2.58	12	7.4	0.06–0.28	2.84 ± 0.02
296	150	10.9	$(COCl)_2$	2.40	23	14	0.15–0.69	2.83 ± 0.03
							Global Fit[b]	2.84 ± 0.02
323	125	15.8	$(COCl)_2$	1.77	26	11	0.13–0.76	2.84 ± 0.04
323	175	11.2	$(COCl)_2$	1.70	18	7.7	0.18–0.62	2.87 ± 0.04
							Global Fit[b]	2.86 ± 0.03
338	125	16.6	$(COCl)_2$	1.51	22	8.2	0.10–0.64	2.85 ± 0.02
338	175	11.7	$(COCl)_2$	1.58	20	7.8	0.10–0.64	2.83 ± 0.03
							Global Fit[b]	2.84 ± 0.02
353	125	8.9	$(COCl)_2$	1.40	26	9.0	0.05–0.19	2.83 ± 0.03
353	125	17.4	$(COCl)_2$	1.43	25	8.9	0.01–0.67	2.82 ± 0.01
353	175	12.3	$(COCl)_2$	1.18	18	5.2	0.09–0.62	2.78 ± 0.05
							Global Fit[b]	2.80 ± 0.02

[a]Quoted uncertainties are 2σ precision of the non-weighted linear least-squares fits with the intercept set to the background loss rate coefficient (k_d).

[b]Global linear least-squares fits (2σ precision) of the combined k(T)-k_d dataset with the intercept fixed to the origin.

TABLE 5 | Summary of experimental conditions and rate coefficients obtained in this work for the Cl + hexamethylcyclotrisiloxane ([-Si$(CH_3)_2$O-]$_3$, D_3) reaction.

				Cl atom source parameters					
T (K)	P (Torr, He)	$[O_2]_0$ (10^{15} molecule cm^{-3})	Linear flow velocity (cm s^{-1})	Cl atom precursor	[Precursor] (10^{14} molecule cm^{-3})	Photolysis laser fluence (mJ cm^{-2} pulse^{-1})	$[Cl]_0$ (10^{11} molecule cm^{-3})	$[D_3]$ Range (10^{14} molecule cm^{-3})	k(T)[a] (10^{-11} cm^3 molecule^{-1} s^{-1})
273	100	7.5	7.1	Cl_2	1.01	8.9	6.1	0.34–2.04	6.41 ± 0.04
273	50	4.5	7.6	Cl_2	0.55	31	9.7	0.12–1.77	6.29 ± 0.05
273	100	5.0	7.7	Cl_2	0.50	21	6.1	0.23–1.43	6.13 ± 0.07
								Global Fit[b]	6.30 ± 0.06
296	100	14.5	6.2	Cl_2	0.84	7.5	4.3	0.33–1.26	5.74 ± 0.07
296	100	14.5	6.2	Cl_2	0.99	15	10.1	0.12–1.26	5.90 ± 0.05
296	50	4.8	8.3	Cl_2	0.58	29	9.6	0.17–1.64	5.56 ± 0.06
296	200	5.0	2.9	Cl_2	0.84	23	11.3	0.19–1.12	6.05 ± 0.14
296	150	-	3.8	$(COCl)_2$	2.66	26	17.1	0.24–1.28	6.19 ± 0.08
296	150	-	4.7	$(COCl)_2$	3.31	23	18.7	0.17–1.21	6.27 ± 0.19
								Global Fit[b]	5.88 ± 0.08
323	50	5.3	9.0	Cl_2	0.62	29	10.3	0.13–1.56	5.78 ± 0.08
323	100	5.8	5.9	Cl_2	0.73	30	12.4	0.12–1.85	5.86 ± 0.08
								Global Fit[b]	5.82 ± 0.06
353	100	7.3	7.3	Cl_2	0.86	8.1	4.8	0.23–1.34	6.00 ± 0.06
353	50	4.5	9.8	Cl_2	0.43	31	7.5	0.12–1.41	6.05 ± 0.07
								Global Fit[b]	6.02 ± 0.05

[a]Quoted uncertainties are 2σ precision of the non-weighted linear least-squares fits with the intercept set to the background loss rate coefficient (k_d).

[b]Global linear least-squares fits (2σ precision) of the combined k(T)-k_d dataset with the intercept fixed to the origin.

TABLE 6 | Summary of experimental conditions and rate coefficients obtained in this work for the Cl + octamethylcyclotetrasiloxane ([-Si(CH_3)$_2$O-]$_4$, D_4) reaction.

				Cl atom source parameters					
T (K)	P (Torr, He)	$[O_2]_0$ (10^{15} molecule cm^{-3})	Linear flow velocity (cm s^{-1})	Cl atom precursor	[Precursor] (10^{14} molecule cm^{-3})	Photolysis laser fluence (mJ cm^{-2} pulse^{-1})	$[Cl]_0$ (10^{11} molecule cm^{-3})	$[D_4]$ Range (10^{14} molecule cm^{-3})	k(T)[a] (10^{-10} cm^3 molecule^{-1} s^{-1})
273	150	—	16.8	$(COCl)_2$	1.22	25	5.7	0.07–0.86	1.19 ± 0.01
273	134	—	15.6	$(COCl)_2$	0.73	20	3.3	0.09–1.25	1.15 ± 0.01
								Global Fit[b]	1.16 ± 0.02
296	50	—	19.8	Cl_2	0.31	32	5.8	0.13–1.06	1.20 ± 0.01
296	50	—	18.2	Cl_2	0.31	32	5.7	0.18–1.07	1.18 ± 0.01
296	50	5.6	19.9	Cl_2	0.31	31	5.5	0.11–1.11	1.16 ± 0.01
296	75	4.1	20.8	Cl_2	0.51	21	7.1	0.15–1.02	1.15 ± 0.01
296	75	5.5	18.2	Cl_2	0.77	23	12	0.08–1.04	1.11 ± 0.01
296	150	—	14.2	$(COCl)_2$	0.93	30	5.2	0.18–1.33	1.12 ± 0.01
296	150	6.2	14.2	$(COCl)_2$	1.11	29	6.0	0.14–1.22	1.12 ± 0.02
296	150	—	10.4	$(COCl)_2$	0.75	28	3.9	0.08–1.16	1.16 ± 0.01
								Global Fit[b]	1.13 ± 0.01
323	100	—	27.2	$(COCl)_2$	0.76	12	12	0.07–1.10	1.15 ± 0.01
323	125	—	17.5	$(COCl)_2$	4.34	25	20	0.10–1.49	1.15 ± 0.01
								Global Fit[b]	1.15 ± 0.01
353	150	—	21.8	$(COCl)_2$	0.74	29	4.0	0.08–0.76	1.15 ± 0.01
353	136	—	20.5	$(COCl)_2$	0.43	26	2.1	0.06–0.87	1.18 ± 0.01
								Global Fit[b]	1.16 ± 0.01

[a]Quoted uncertainties are 2σ precision of the non-weighted linear least-squares fits with the intercept set to the background loss rate coefficient (k_d).

[b]Global linear least-squares fits (2σ precision) of the combined k(T)-k_d dataset with the intercept fixed to the origin.

TABLE 7 | Summary of experimental conditions and rate coefficients obtained in this work for the Cl + decamethylcyclopentasiloxane ([-Si(CH_3)$_2$O-]$_5$, D_5) reaction.

				Cl atom source parameters					
T (K)	P (Torr,He)	$[O_2]_0$ (10^{15} molecule cm^{-3})	Linear flow velocity (cm s^{-1})	Cl atom precursor	[Precursor] (10^{14} molecule cm^{-3})	Photolysis laser fluence (mJ cm^{-2} pulse^{-1})	$[Cl]_0$ (10^{11} molecule cm^{-3})	[D_5] Range (10^{14} molecule cm^{-3})	k(T)[a] (10^{-10} cm^3 molecule^{-1} s^{-1})
273	125	9.5	5.6	Cl_2	0.81	15	8.1	0.21–1.19	1.73 ± 0.01
273	124	-	5.7	$(COCl)_2$	1.75	18	4.0	0.11–0.78	1.71 ± 0.03
273	125	-	11.1	$(COCl)_2$	2.72	20	14	0.14–0.90	1.75 ± 0.02
								Global Fit[b]	1.73 ± 0.02
296	200	10	4.4	Cl_2	0.54	18	6.7	0.13–0.95	1.66 ± 0.01
296	50	9.3	10.2	Cl_2	0.22	16	2.4	0.26–1.29	1.73 ± 0.01
296	100	9.0	8.8	Cl_2	0.30	14	2.7	0.19–1.12	1.75 ± 0.01
296	100	8.4	6.3	Cl_2	0.88	24	8.8	0.12–0.96	1.70 ± 0.02
296	125	-	7.9	$(COCl)_2$	2.14	9.2	2.5	0.13–1.16	1.73 ± 0.02
296	200	-	5.5	$(COCl)_2$	2.80	4.8	1.7	0.08–1.12	1.74 ± 0.03
296	124	-	10.3	$(COCl)_2$	1.59	20	3.9	0.13–0.84	1.75 ± 0.02
								Global Fit[b]	1.72 ± 0.01
323	150	9.6	5.6	Cl_2	0.65	19	9.6	0.20–1.23	1.73 ± 0.02
323	150	10	6.4	Cl_2	0.69	12	7.1	0.19–1.15	1.74 ± 0.05
323	124	-	7.7	$(COCl)_2$	1.48	17	3.2	0.10–0.98	1.74 ± 0.02
								Global Fit[b]	1.74 ± 0.01
353	100	8.6	8.2	Cl_2	1.00	44	4.3	0.14–1.06	1.67 ± 0.02
353	125	-	18.4	$(COCl)_2$	1.40	18	6.2	0.09–0.62	1.72 ± 0.02
353	125	-	12.1	$(COCl)_2$	2.27	22	13	0.09–0.86	1.68 ± 0.02
								Global Fit[b]	1.68 ± 0.01

[a]Quoted uncertainties are 2σ precision of the non-weighted linear least-squares fits with the intercept set to the background loss rate coefficient (k_d).

[b]Global linear least-squares fits (2σ precision) of the combined k(T)-k_d dataset with the intercept fixed to the origin.

TABLE 8 | Summary of experimental conditions and rate coefficients obtained in this work for the dodecamethylcyclohexasiloxane ([-Si$(CH_3)_2$O-]$_6$, D_6) reaction.

			Cl atom source parameters					
T (K)	P (Torr, He)	Linear flow velocity (cm s^{-1})	Cl atom precursor	[Precursor] (10^{14} molecule cm^{-3})	Photolysis laser fluence (mJ cm^{-2} $pulse^{-1}$)	$[Cl]_0$ (10^{11} molecule cm^{-3})	$[D_6]$ Range (10^{14} molecule cm^{-3})	k(T)[a] (10^{-10} cm^3 $molecule^{-1}$ s^{-1})
296	125	12.6	$(COCl)_2$	1.34	23	7.5	0.05–0.42	2.19 ± 0.02
296	150	8.7	$(COCl)_2$	1.87	23	10.5	0.07–0.50	2.19 ± 0.01
							Global Fit[b]	2.19 ± 0.01
323	150	9.6	$(COCl)_2$	1.96	23	9.4	0.09–0.55	2.13 ± 0.03
323	175	8.1	$(COCl)_2$	1.87	20	9.1	0.11–0.61	2.18 ± 0.01
							Global Fit[b]	2.16 ± 0.02
338	125	17.4	$(COCl)_2$	1.27	19	6.1	0.10–0.42	2.12 ± 0.01
338	175	8.5	$(COCl)_2$	0.83	19	3.9	0.08–0.56	2.15 ± 0.02
							Global Fit[b]	2.14 ± 0.02
353	175	10.1	$(COCl)_2$	1.09	21	5.6	0.11–0.52	2.09 ± 0.03
353	125	12.0	$(COCl)_2$	1.26	18	5.7	0.09–0.56	2.08 ± 0.03
							Global Fit[b]	2.09 ± 0.02

[a]Quoted uncertainties are 2σ precision of the non-weighted linear least-squares fits with the intercept set to the background loss rate coefficient (k_d).

[b]Global linear least-squares fits (2σ precision) of the combined k(T)-k_d dataset with the intercept fixed to the origin.

TABLE 9 | Comparison of the Arrhenius parameters and 296 K rate coefficients for the Cl + permethyl siloxane (PMS) reactions obtained in this work and literature values.

PMS	T Range (K)	Pressure (Torr)	Kinetic method: Detection method[c]	Arrhenius parameters		Relative rate (RR) reference compound	k(296 K)[b] (10^{-10} cm^3 molecule^{-1} s^{-1})	Reference
				A[a,b] (10^{-10} cm^3 molecule^{-1} s^{-1})	E/R (T)			
L_2	273–363	50–200	PLP:RF	1.36 ± 0.10	43 ± 249	—	1.58 ± 0.07	This work
	296 ± 2	~760	RR: PTR-ToF MS	—	—	Isoprene	1.31 ± 0.21	Geetha et al. [19]
						Toluene	0.95 ± 0.14	
	297 ± 3	~645	RR:ToF-CIMS	—	—	MEK[x]	1.5 ± 0.5	Alton and Browne [17]
						Et_2O [y]	1.39 ± 0.05	
							1.44 ± 0.05	
	297 ± 2	~740	RR:GC-FID	—	—	n-butane	1.46 ± 0.3	Atkinson et al. [14]
	273–363	~0.002	Knudsen Cell: MS	0.916 ± 0.038	11 ± 136	—	1.00 ± 0.19	Prosmitis et al. [18]
L_3	273–353	50–150	PLP:RF	1.95 ± 0.18	1 ± 632	—	1.93 ± 0.09	This work
	296 ± 2	~760	RR:PTR-ToF MS	—	—	Isoprene	1.56 ± 0.23	Geetha et al. [19]
						Toluene	1.35 ± 0.16	
	297 ± 3	~645	RR:ToF-CIMS	—	—	MEK	1.9 ± 0.5	Alton and Browne [17]
						Et_2O	1.77 ± 0.06	
							1.85 ± 0.05	
L_4	273–353	125–250	PLP:RF	2.09 ± 0.16	43 ± 522	—	2.36 ± 0.12	This work
	296 ± 2	~760	RR:PTR-ToF MS	—	—	Isoprene	1.98 ± 0.29	Geetha et al. [19]
						Toluene	1.43 ± 0.14	
	297 ± 3	~645	RR:ToF-CIMS	—	—	MEK	2.3 ± 0.5	Alton and Browne [17]
						Et_2O	2.1 ± 0.1	
							2.2 ± 0.1	
L_5	296–353	125–175	PLP:RF	2.70 ± 0.18	15 ± 490	—	2.84 ± 0.19	This work
	296 ± 2	~760	RR:PTR-ToF MS	—	—	Isoprene	2.22 ± 0.34	Geetha et al. [19]
						Toluene	2.14 ± 0.22	
	297 ± 3	~645	RR:ToF-CIMS	—	—	MEK	2.9 ± 0.5	Alton and Browne [17]
						Et_2O	2.8 ± 0.4	
							2.9 ± 0.1	

(Continues)

TABLE 9 | (Continued)

PMS	T Range (K)	Pressure (Torr)	Kinetic method: Detection method[c]	Arrhenius parameters		Relative rate (RR) reference compound	k(296 K)[b] (10^{-10} cm^3 molecule^{-1} s^{-1})	Reference
				A[a,b] (10^{-10} cm^3 molecule^{-1} s^{-1})	E/R (T)			
D_3	273–353	50–200	PLP:RF	0.47 ± 0.03	78 ± 470	—	0.588 ± 0.028	This work
	296 ± 2	~760	R:PTR-ToF MS	—	—	Isoprene	0.56 ± 0.13	Geetha et al. [19]
						Toluene	0.52 ± 0.05	
	297 ± 3	~645	RR:ToF-CIMS	—	—	MEK	0.57 ± 0.05	Alton and Browne [17]
						Et_2O	0.5 ± 0.1	
							0.56 ± 0.05	
D_4	273–353	50–150	PLP:RF	1.14 ± 0.07	4 ± 432	—	1.13 ± 0.06	This work
	296 ± 2	~760	RR:PTR-ToF MS	—	—	Isoprene	1.05 ± 0.16	Geetha et al. [19]
						Toluene	0.89 ± 0.11	
	297 ± 3	~645	RR:ToF-CIMS	—	—	MEK	1.14 ± 0.08	Alton and Browne [17]
						Et_2O	1.39 ± 0.05	
							1.16 ± 0.06	
D_5	273–353	50–200	PLP-RF	1.60 ± 0.10	22 ± 432	—	1.72 ± 0.09	This work
	296 ± 2	~760	RR:PTR-ToF MS	—	—	Isoprene	1.46 ± 0.22	Geetha et al. [19]
						Toluene	1.21 ± 0.15	
	297 ± 3	~645	RR:ToF-CIMS	—	—	MEK	1.8 ± 0.2	Alton and Browne [17]
						Et_2O	1.8 ± 0.2	
							1.8 ± 0.1	
D_6	296–353	125–175	PLP:RF	1.73 ± 0.14	71 ± 562	—	2.16 ± 0.14	This work
	296 ± 2	~760	RR:PTR-ToF MS	—	—	Isoprene	1.61 ± 0.25	Geetha et al. [19]
						Toluene	1.52 ± 0.17	

[a]Arrhenius parameters obtained from a 2σ weighted linear least-squares fit of the experimental data in Tables 1–8.

[b]Literature uncertainties in k(296 K) are 2σ, except for Sarachandra Kumar Geetha et al. who report 1σ uncertainties. Uncertainties in the k(296 K) from this work are absolute uncertainties including estimated systematic errors.

[c]Methods: PLP, Pulsed Laser Photolysis; RF, Resonance Fluorescence; ToF, time-of-flight; CIMS, Chemical Ionization Mass Spectrometry; PTR, Proton Transfer; MS, Mass Spectrometry, MEK: methyl ethyl ketone, $(CH_3)_2C(O)CH_2CH_3$; Et_2O, diethyl ether: $CH_3CH_2OCH_2CH_3$

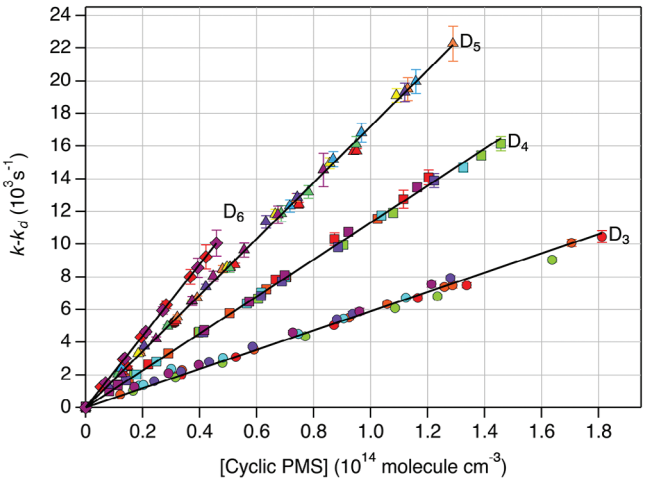

FIGURE 4 | Rate coefficient data (k-k_d) for the Cl atom + cyclic permethylsiloxane (PMS) reactions measured in this work at 296 K: hexamethylcyclotrisiloxane ([-Si$(CH_3)_2$O-]$_3$, D_3 (circles); octamethylcyclotetrasiloxane ([-Si$(CH_3)_2$O-]$_4$, D_4 (squares), decamethylcyclopentasiloxane ([-Si$(CH_3)_2$O-]$_5$, D_5 (triangles), dodecamethylcyclohexasiloxane ([-Si$(CH_3)_2$O-]$_6$, D_6 (diamonds)) reaction (see Tables 5–8). The lines are linear least-squares fits of the combined datasets. Individual experiments are denoted by different marker colors. The data error bars are 2σ of the linear least-squares fit of the Cl atom decay.

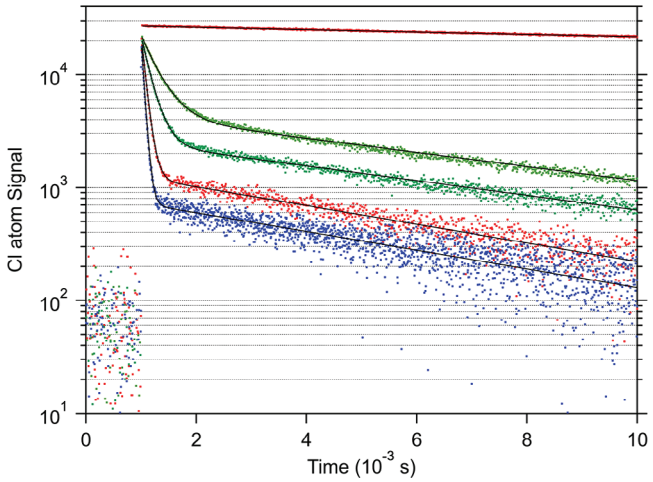

FIGURE 5 | Representative Cl atom temporal profiles obtained for the Cl + hexamethyldisiloxane (HMDS) ($(CH_3)_3SiOSi(CH_3)_3$, L_2) reaction at 296 K and 100 Torr (He) with Cl_2 (~6.7×10^{13} molecule cm^{-3}) as the Cl atom precursor, see Table S1. L_2 concentrations from top to bottom profile are (10^{13} molecule cm^{-3}): 0.0, 1.46, 2.75, 6.14, and 9.59. Profiles are background corrected. Profiles obtained with L_2 concentrations of 4.41, 8.67, and 14.6 are not included for clarity. The lines are non-linear bi-exponential least-squares fits of the data (see Table S1).

illustrates the consistency of the measurements across a range of [PMS].

Rate coefficient results given in Tables 1–8 and shown in Figures 3 and 4 demonstrate that all the studied reactions were independent of the experimental conditions, including linear flow velocity through the reactor, the photolysis laser fluence and wavelength, and initial Cl atom concentration, $[Cl]_0$. In addition, rate coefficients obtained for L_2 and L_3 and D_3, D_4, and D_5 (see Tables 1, 2, 5, 6, and 7) using the Cl atom precursors $(COCl)_2$ and Cl_2, with O_2 present in large excess, $>4 \times 10^{15}$ molecule cm^{-3}, agreed to within the measurement precision. Measurements with the Cl_2 precursor in the absence of O_2 are discussed later. Measurements using $(COCl)_2$ with and without the addition of O_2 yielded identical rate coefficient results. Preferred rate coefficients were obtained using the $(COCl)_2$ source, which showed single exponential decay under all experimental conditions and improved Cl atom sensitivity due to the absence of fluorescence quenching by O_2. The Cl + L_4, L_5, and D_6 reactions were measured only using $(COCl)_2$ as the Cl atom source.

The potential impact of excited spin-state Cl atoms, $Cl(^2P_{1/2})$, on the measured rate coefficients was examined in a few experiments, see Table 1. SF_6 was added to quench any spin excited Cl atoms to the ground state $Cl(^2P_{3/2})$ [37]:

$$SF_6 + Cl\left(^2P_{1/2}\right) \rightarrow SF_6 + Cl\left(^2P_{3/2}\right) \quad (13)$$

where $k_{13} = 1.5 \times 10^{-10}$ molecule cm^{-3} s^{-1} [38]. Under the experimental conditions used, 99% of $Cl(^2P_{1/2})$ would have been quenched to $Cl(^2P_{3/2})$ within ~2 μs. Rate coefficients measured for Reaction (1) with and without the addition of SF_6 were identical to within the measurement precision. We assume that this applies to all the other reactions studied.

5 | Radical Scavenging

Figure 5 shows a representative set of Cl atom temporal profiles obtained at 296 K for the Cl + L_2 reaction in the absence of added radical scavengers (He bath gas). The bi-exponential decay behavior is consistent with Cl atom regeneration and was observed in all experiments where Cl_2 was used as the Cl photolysis source in the absence of added radical scavengers (see Table S1). Cl atom regeneration is assumed to occur from Reaction (11), resulting in the formation of a chlorinated PMS product and a Cl atom.

The influence of the Cl_2 + PMS product reaction pathway was effectively minimized by the addition of O_2 to scavenge the PMS radical products via peroxy radical formation, resulting in Cl atom single exponential decay profiles. In experiments conducted without added O_2 (see Table S1), the slower component of the decay varied between 100 and 300 s^{-1}. For the measurement shown in Figure 5, $[Cl_2] \gg$ [PMS radical], the rate coefficient of the Cl_2 + PMS radical reaction is estimated to be ~2.9×10^{-12} cm^3 molecule^{-1} s^{-1} at 296 K. Figure 6 (**upper**) shows that $[O_2] \geq 10^{15}$, that is, ~15 times greater than the $[Cl_2]$, is sufficient to suppress the secondary Cl atom generation in the Cl + hexamethylcyclotrisiloxane ([-Si$(CH_3)_2$O-]$_3$, D_3) reaction.

The rate coefficient for the reaction of the D_3 radical product with O_2 was measured in two separate experiments at 296 K and 100 Torr total pressure (He bath gas). The D_3 concentration was held constant and the O_2 concentration varied between 0.22 and 1.43 (10^{15}) molecule cm^{-3}. The profiles shown in Figure 6 (**upper**) show an increase in Cl atom loss with increasing O_2 concentration. A second-order plot of the PMS radical first-order loss versus $[O_2]$ yielded $k_{12}(296\ K) = (1.80 \pm 0.14) \times 10^{-12}$ cm^3 molecule^{-1} s^{-1} where the uncertainty is the 2σ precision of the fit (Figure 6, **lower**). For the measurements in Tables 1, 2, and 5–7

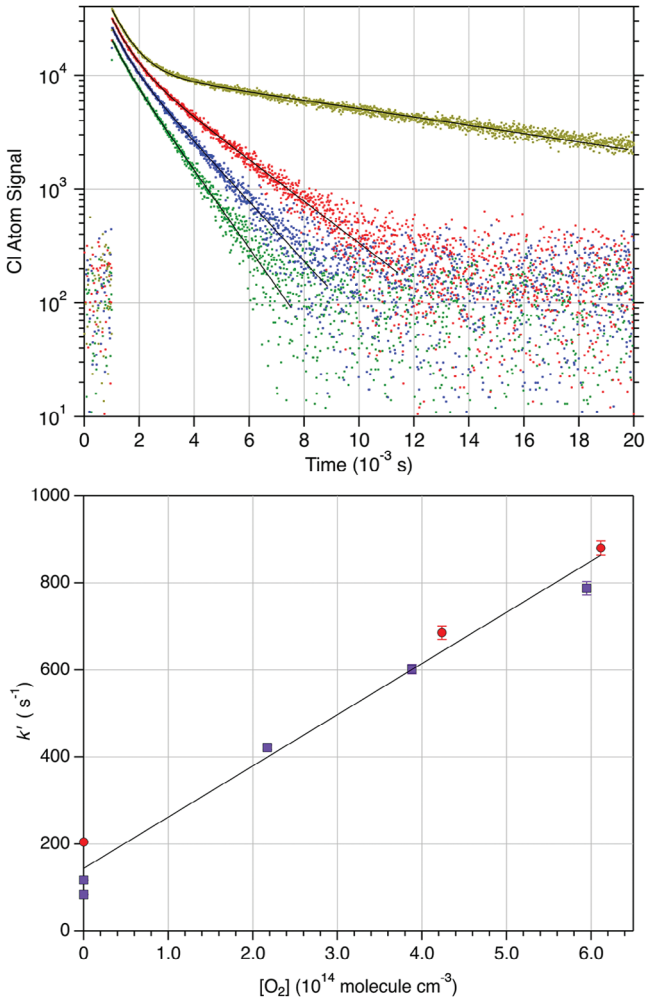

FIGURE 6 | Upper: Representative Cl atom decay profiles (offset for clarity) obtained using the Cl_2 precursor with increasing [O_2]. Experimental conditions: Total Pressure = 100 Torr (He bath gas), 296 K, [Cl_2] = 9.20×10^{13} molecule cm^{-3}, Photolysis Laser Fluence = 9 mJ cm^{-2} $pulse^{-1}$; $[Cl]_0 = 5.6 \times 10^{11}$ atom cm^{-3}; [D_3] = 1.85×10^{13} molecule cm^{-3}. [O_2] from top to bottom profile are 0, 2.2, 3.9, 5.9 (10^{14} molecule cm^{-3}). Lower: Second order plot, k' versus [O_2], from two independent measurements (circles and squares), where k' was taken from the 2nd (slower) decay obtained from a bi-exponential fit of the Cl atom profile. The line is a least-squares fit to the combined dataset.

where Cl_2/O_2 a source/scavenger method was used, the minimum [O_2]/[Cl_2] ratio was ~31.

6 | Experimental Uncertainties

The absolute uncertainty in the recommended rate coefficients is estimated from the random and estimated systematic errors in our measurements. The precision of the linear least squares fits of k'(T) versus [PMS] were better than 3% for all PMSs studied. Systematic errors in the measurements include the temperature measurement (1 K), pressure measurement (1%), and uncertainties in the measurement infrared cross sections of L_2 (2%), L_3 (2%), L_4 (3%), L_5 (5%), D_3 (2%), D_4 (3%), D_5 (3%), and D_6 (5%) [36]. The [PMS] used in the kinetic analysis was an average of two FTIR spectra, which typically agreed to within 2%.

The precision of the k' determinations was better than 4%. The recommended rate coefficients (in units of 10^{-10} cm^3 $molecule^{-1}$ s^{-1}) for the Cl + PMS reactions are:

L_2k_1 (296 K) = (1.58 ± 0.07)	D_3k_5 (296 K) = (0.588 ± 0.028)
L_3k_2 (296 K) = (1.93 ± 0.09)	D_4k_6 (296K) = (1.13 ± 0.06)
L_4k_3 (296 K) = (2.36 ± 0.12)	D_5k_7 (296K) = (1.72 ± 0.09)
L_5k_4 (296 K) = (2.84 ± 0.19)	D_6k_8 (296K) = (2.16 ± 0.14)

where the quoted absolute uncertainties are 2σ.

This study further demonstrates the different reactivity of cyclic and linear PMS, where the linear PMS is more reactive than the cyclic PMS analog containing the same number of methyl groups, for example, L_2 and D_3. This has been observed in previous investigations for both the OH + PMS [10, 13, 17, 19] and Cl + PMS [14, 17–19] reactions. In this study, the cyclic and linear PMS rate coefficients were found to increase linearly with an increasing number of methyl groups. The reaction rate coefficient increased by (2.1 ± 0.2) × 10^{-11} and (2.7 ± 0.2) × 10^{-11} cm^3 $molecule^{-1}$ s^{-1} per methyl group added for linear and cyclic PMS, respectively. The trend in reactivity can be expressed as a structure activity relationship (SAR), using the methods developed by Atkinson and coworkers [39–41], where the observed rate coefficient is expressed as the sum of the reactive sites:

$$k_{\text{Observed}} = \sum (N_{CH_3} \times k_{\text{prim}} \times F(\text{X}))$$

where N_{CH3} is the number of CH_3-groups in the molecule, k_{prim} is the representative Cl + CH_3- group rate coefficient, 3.5 ×10^{-11} cm^3 $molecule^{-1}$ s^{-1} [42], and F(X) is the enhancement factor for the chemical environment, X. Although the CH_3- groups in the linear and cyclic PMSs have slightly different chemical environments, all the CH_3- groups were assumed to have the same enhancement factor, (the fit results justify the assumption). Atkinson [41] has shown that including a multiplicative ring-strain enhancement factor, F_{Ring}, for cyclic compounds accounts for the smaller rate coefficients observed for *cyclo*-alkanes. We have applied individual F_{Ring} factors for the cyclic $D_{3\text{-}6}$ PMSs. First, the linear compounds were fit with an F(X) value of 0.69. The SAR fit reproduces the $L_{2\text{-}5}$ PMS rate coefficients to better than ~11%, see Figure S10. Next, F_{Ring} was optimized for each individual cyclic PMS. F_{Ring} values of 0.41, 0.59, 0.71, and 0.76 were obtained for D_3, D_4, D_5, and D_6, respectively. The fits are shown in Figure S11 reproduce the Cl atom rate coefficients obtained in this work to within 5%, or better. F_{Ring} increased, that is, less ring-strain (see geometries given in Figure S1), with increasing PMS ring size. The increase in F_{Ring} with increasing ring size asymptotically approaches unity, although parameterization of the trend is not warranted given such a small dataset. Note, that the absolute values of F_{Ring} depend on the choice of k_{prim}, that is, a lower value of k_{prim} would lead to greater values of F_{Ring}, although the trend with ring size would remain.

7 | Literature Comparison

A comparison of the kinetic results for the Cl + PMS reactions in this work and reported previously is provided in Table 9. To the best of our knowledge, this study is the first to systematically explore Cl + PMS reactivity over a range of temperatures using an

absolute kinetic method. The rate coefficients for the Cl + PMS reactions were found to be nearly independent of temperature over the range of temperatures included in this study. Rate coefficient measurement in a previous study by Promisitis et al. [18] for the Cl + L_2 reaction at temperatures between 273 and 363 K were also found to be temperature independent. Our measured rate coefficients for Cl + L_2, however, are systematically ∼37% greater than that of Promisitis et al. [18]. All previous relative rate measurements were performed at room temperature, 297 ± 3 K. For the Cl + L_2 reaction, the reported rate coefficients are slightly less than our work, but within the combined uncertainties of the measurements; the Cl + L_2 reaction rate coefficient reported by Alton and Browne [17] has the largest deviation (9.3%) from our k(296 K). On average, the rate coefficients reported by Alton and Browne are within ∼5% of our measured values for the linear PMSs except for L_2.

A comparison of the Cl + cyclic PMS rate coefficients shows that the spread in the measured rate coefficients among the three available studies shown in Table 9 is less than that for the linear PMSs. As the size of the PMS increases, the spread in the measured rate coefficients increases, with the values of Geetha et al. [19] always systematically lower than the values of Alton and Browne and those obtained in this work. The relative rate weighted average k(296 K) values reported by Alton and Browne are in excellent agreement with the absolute k(296 K) measured in this work, with a maximum deviation of 4.9% for the Cl + D_3 reaction. Overall, Table 9 shows that there is reasonable agreement among the Cl + PMS room temperature rate coefficient data, while the estimated absolute uncertainty is significantly reduced in the present study.

8 | Summary

Using a PLP-RF absolute kinetic method, we have measured Cl + PMS reaction rate coefficients of the four smallest linear and cyclic PMSs L_2, L_3, L_4, L_5, D_3, D_4, D_5, and D_6 over range of temperature (273–353 K) and pressure (50–250 Torr, He bath gas), see Tables 1–8. The present measurements yielded rate coefficient data of high precision and accuracy with estimated 2σ absolute uncertainties of ∼7%.

Rate coefficients for the Cl + PMS reactions are ∼100 fold more reactive than the OH radical [15, 20]. The relative contribution of the Cl atom reaction to the atmospheric lifetime and degradation of PMSs hinges on the atmospheric abundance of Cl atoms, which is highly spatially and temporally variable. The atmospheric abundance of Cl atoms has been found to be elevated in some indoor, coastal, and urban areas [43]. Activation and enhanced Cl atom abundance has been attributed to local sources, for example, in urban photolysis of chloramines (NH_2Cl, $NHCl_2$ and NCl_3) [44], photolysis of particulate nitrate [45], BrCl photolysis [46], and from the use of chlorinated cleaning products [47, 48].

For a Cl atom concentration of ∼1 × 10^4 atom cm^{-3}, inferred from previous studies in a variety of environments [43–46, 48–52], the loss of PMS due to Cl atom reaction yields lifetimes of 7, 6, 5, 4, 20, 10, 7, and 5 days for L_2, L_3, L_4, L_5, D_3, D_4, D_5, and D_6, respectively. For these conditions, the Cl atom reaction approximately represents 50, 50, 30, 30, 85, 80, 60, and 60% of the combined loss due to OH radical (given [OH] ≈ 1.2 × 10^6 molecule cm^{-3} [53]) and Cl atom reactive loss for L_2, L_3, L_4, L_5, D_3, D_4, D_5, and D_6, respectively. Therefore, the Cl chemistry of PMSs needs to be included in local and regional air quality forecast models, especially in urban coastal areas where the co-location of PMS and reactive Cl is likely to be high. The ubiquity of siloxanes and the importance of the chlorine atom in driving their atmospheric transformations underscores the relevance of thoroughly characterizing siloxane chemistry for elucidating air quality across diverse environments.

Data Availability Statement

The data that supports the findings of this study are available in the supplementary material of this article

References

1. S. Genualdi, T. Harner, Y. Cheng, et al., "Global Distribution of Linear and Cyclic Volatile Methyl Siloxanes in Air," *Environmental Science & Technology* 45 (2011): 3349–3354.

2. C. E. Brunet, R. F. Marek, C. O. Stanier, and K. C. Hornbuckle, "Concentrations of Volatile Methyl Siloxanes in New York City Reflect Emissions From Personal Care and Industrial Use," *Environmental Science & Technology* 58 (2024): 8835–8845.

3. X. Tang, P. K. Misztal, W. W. Nazaroff, and A. H. Goldstein, "Siloxanes Are the Most Abundant Volatile Organic Compound Emitted From Engineering Students in a Classroom," *Environmental Science & Technology Letters* 2 (2015): 303–307.

4. M. M. Coggon, B. C. McDonald, A. Vlasenko, et al., "Diurnal Variability and Emission Pattern of Decamethylcyclopentasiloxane (D5) From the Application of Personal Care Products in Two North American Cities," *Environmental Science & Technology* 52 (2018): 5610–5618.

5. S. Xu, N. Warner, P. Bohlin-Nizzetto, J. Durham, and D. McNett, "Long-Range Transport Potential and Atmospheric Persistence of Cyclic Volatile Methylsiloxanes Based on Global Measurements," *Chemosphere* 228 (2019): 460–468.

6. J. Kim, D. Mackay, and M. J. Whelan, "Predicted Persistence and Response Times of Linear and Cyclic Volatile Methylsiloxanes in Global and Local Environments," *Chemosphere* 195 (2018): 325–335.

7. F. Wania, N. A. Warner, M. S. McLachlan, et al., "Seasonal and Latitudinal Variability in the Atmospheric Concentrations of Cyclic Volatile Methyl Siloxanes in the Northern Hemisphere," *Environmental Science: Processes & Impacts* 25 (2023): 496–506.

8. J. Jiang, X. Ding, S. S. Patra, et al., "Siloxane Emissions and Exposures During the Use of Hair Care Products in Buildings," *Environmental Science & Technology* 57 (2023): 19999–20009.

9. J. Kim and S. Xu, "Quantitative Structure-Reactivity Relationships of Hydroxyl Radical Rate Constants for Linear and Cyclic Volatile Methylsiloxanes," *Environmental Toxicology and Chemistry* 36 (2017): 3240–3245.

10. S. J. Markgraf and J. R. Wells, "The Hydroxyl Radical Reaction Rate Constants and Atmospheric Reaction Products of Three Siloxanes," *International Journal of Chemical Kinetics* 29 (1997): 445–451.

11. A. Safron, M. Strandell, A. Kierkegaard, and M. Macleod, "Rate Constants and Activation Energies for Gas-Phase Reactions of Three Cyclic Volatile Methyl Siloxanes With the Hydroxyl Radical," *International Journal of Chemical Kinetics* 47 (2015): 420–428.

12. R. Sommerlade, H. Parlar, D. Wrobel, and P. Kochs, "Product Analysis and Kinetics of the Gas-Phase Reactions of Selected Organosilicon Compounds With OH Radicals Using a Smog Chamber-Mass Spectrometer System," *Environmental Science & Technology* 27 (1993): 2435–2440.

13. R. Atkinson, "Kinetics of the Gas-Phase Reactions of a Series of Organosilicon Compounds With Hydroxyl and Nitrate(NO_3) Radicals and Ozone at 297 ± 2 K," *Environmental Science & Technology* 25 (1991): 863–866.

14. R. Atkinson, E. C. Tuazon, E. S. C. Kwok, J. Arey, S. M. Aschmann, and I. Bridier, "Kinetics and Products of the Gas-Phase Reactions of $(CH_3)_4Si$, $(CH_3)_3SiCH_2OH$, $(CH_3)_3SiOSi(CH_3)_3$ and $(CD_3)_3SiOSi(CD_3)_3$ With Cl Atoms and OH Radicals," *Journal of the Chemical Society, Faraday Transactions* 91 (1995): 3033–3039.

15. F. Bernard, D. K. Papanastasiou, V. C. Papadimitriou, and J. B. Burkholder, "Temperature Dependent Rate Coefficients for the Gas-Phase Reaction of the OH Radical With Linear (L2, L3) and Cyclic (D3, D4) Permethylsiloxanes," *Journal of Physical Chemistry A* 122 (2018): 4252–4264.

16. R. Xiao, I. Zammit, Z. Wei, W.-P. Hu, M. MacLeod, and R. Spinney, "Kinetics and Mechanism of the Oxidation of Cyclic Methylsiloxanes by Hydroxyl Radical in the Gas Phase: An Experimental and Theoretical Study," *Environmental Science & Technology* 49 (2015): 13322–13330.

17. M. W. Alton and E. C. Browne, "Atmospheric Chemistry of Volatile Methyl Siloxanes: Kinetics and Products of Oxidation by OH Radicals and Cl Atoms," *Environmental Science & Technology* 54 (2020): 5992–5999.

18. A. V. Prosmitis, V. C. Papadimitriou, J. Pola, and P. Papagiannakopoulos, "Kinetic Study for the Reactions of Chlorine Atoms With Hexamethyldisiloxane, 1,1,3,3-Tetramethyldisiloxane, and 1,3-Dimethyldisiloxane," *Chemical Physics Letters* 344 (2001): 241–248.

19. A. S. K. Geetha, T. Mikoviny, F. Piel, and A. Wisthaler, "Room Temperature Rate Coefficients for the Reaction of Chlorine Atoms With a Series of Volatile Methylsiloxanes (L2-L5, D3-D6)," *International Journal of Chemical Kinetics* 55 (2023): 570–576.

20. F. Bernard and J. B. Burkholder, "Rate Coefficients for the Gas-Phase Reaction of OH Radicals With the L4, L5, D5, and D6 Permethylsiloxanes," *Submitted IJCK* (2024).

21. M. W. Alton, V. L. Johnson, S. Sharma, and E. C. Browne, "Volatile Methyl Siloxane Atmospheric Oxidation Mechanism From a Theoretical Perspective — How Is the Siloxanol Formed?" *Journal of Physical Chemistry A* 127 (2023): 10233–10242.

22. A. M. Avery, M. W. Alton, M. R. Canagaratna, et al., "Comparison of the Yield and Chemical Composition of Secondary Organic Aerosol Generated From the OH and Cl Oxidation of Decamethylcyclopentasiloxane," *ACS Earth and Space Chemistry* 7 (2023): 218–229.

23. Y. Chen, Y. Park, H. G. Kang, J. Jeong, and H. Kim, "Chemical Characterization and Formation of Secondary Organosiloxane Aerosol (SOSiA) From OH Oxidation of Decamethylcyclopentasiloxane," *Environmental Science: Atmospheres* 3 (2023): 662–671.

24. C. Han, H. Yang, K. Li, et al., "Secondary Organic Aerosols From OH Oxidation of Cyclic Volatile Methyl Siloxanes as an Important Si Source in the Atmosphere," *Atmospheric Chemistry and Physics* 22 (2022): 10827–10839.

25. H. G. Kang, Y. Chen, Y. Park, T. Berkemeier, and H. Kim, "Volatile Oxidation Products and Secondary Organosiloxane Aerosol From D_5 + OH at Varying OH Exposures," *Atmospheric Chemistry and Physics* 23 (2023): 14307–14323.

26. J. N. Meepage, J. K. Welker, C. M. Meyer, S. Mohammadi, C. O. Stanier, and E. A. Stone, "Advances in the Separation and Detection of Secondary Organic Aerosol Produced by Decamethylcyclopentasiloxane (D_5) in Laboratory-Generated and Ambient Aerosol," *ACS EST Air* 1 (2024): 365–375.

27. Y. Wu and M. V. Johnston, "Aerosol Formation From OH Oxidation of the Volatile Cyclic Methyl Siloxane (cVMS) Decamethylcyclopentasiloxane," *Environmental Science & Technology* 51 (2017): 4445–4451.

28. P. Yao, R. Holzinger, D. Materić, et al., "Methylsiloxanes From Vehicle Emissions Detected in Aerosol Particles," *Environmental Science & Technology* 57 (2023): 14269–14279.

29. A. Chattopadhyay, T. Gierczak, P. Marshall, V. C. Papadimitriou, and J. B. Burkholder, "Kinetic Fall-Off Behavior for the Cl + Furan-2,5-dione ($C_4H_2O_3$, maleic anhydride) Reaction," *Physical Chemistry Chemical Physics* 23 (2021): 4901–4911.

30. T. Gierczak, D. K. Papanastasiou, and J. B. Burkholder, "Reaction of Cl Atom With c-C_5F_8 and c-C_5HF_7: Relative and Absolute Measurements of Rate Coefficients and Identification of Degradation Products," *Journal of Physical Chemistry A* 126 (2022): 7737–7749.

31. D. K. Papanastasiou and J. B. Burkholder, "Rate Coefficients for the $O(^3P)$ + Cl_2O Gas-Phase Reaction Between 230 and 357 K," *International Journal of Chemical Kinetics* 43 (2011): 312–321.

32. B. Ghosh, D. K. Papanastasiou, and J. B. Burkholder, "Oxalyl Chloride, ClC(O)C(O)Cl: UV/Vis Spectrum and Cl Atom Photolysis Quantum Yields at 193, 248, and 351 Nm," *Journal of Chemical Physics* 137 (2012).

33. J. M. Nicovich, K. D. Kreutter, and P. H. Wine, "Kinetics and Thermochemistry of ClCO Formation From the Cl + CO Association Reaction," *Journal of Chemical Physics* 92 (1990): 3539–3544.

34. J. B. Burkholder, S. P. Sander, J. Abbatt, et al., *JPL Publication 19-5* (Pasadena: Jet Propulsion Laboratory, 2019), http://jpldataeval.jpl.nasa.gov.

35. D. Davis and W. Braun, "Intense Vacuum Ultraviolet Atomic Line Sources," *Applied Optics* 7 (1968): 2071–2074.

36. F. Bernard, D. K. Papanastasiou, V. C. Papadimitriou, and J. B. Burkholder, "Infrared Absorption Spectra of Linear (L2–L5) and Cyclic (D3–D6) Permethylsiloxanes," *Journal of Quantitative Spectroscopy and Radiative Transfer* 202 (2017): 247–254.

37. M. Ahmed, D. Blunt, D. Chen, and A. G. Suits, "UV Photodissociation of Oxalyl Chloride Yields Four Fragments From One Photon Absorption," *Journal of Chemical Physics* 106 (1997): 7617–7624.

38. S. A. Sotnichenko, V. C. Bokun, and A. I. Nadkhin, "Collisional Quenching of Chlorine (3^2P_{12}) by H_2, D_2, CO, O_2, N_2 and CO_2," *Chemical Physics Letters* 153 (1988): 560–568.

39. R. Atkinson, "A Structure-Activity Relationship for the Estimation of Rate Constants for the Gas-Phase Reactions of OH Radicals With Organic Compounds," *International Journal of Chemical Kinetics* 19 (1987): 799–828.

40. R. Atkinson, "Kinetics and Mechanisms of the Gas-Phase Reactions of the Hydroxyl Radical With Organic Compounds Under Atmospheric Conditions," *Chemical Reviews* 86 (1986): 69–201.

41. E. S. C. Kwok and R. Atkinson, "Estimation of Hydroxyl Radical Reaction Rate Constants for Gas-Phase Organic Compounds Using a Structure-Reactivity Relationship: An Update," *Atmospheric Environment* 29 (1995): 1685–1695.

42. R. Atkinson, "Gas-Phase Tropospheric Chemistry of Volatile Organic Compounds: 1. Alkanes and Alkenes," *Journal of Physical and Chemical Reference Data* 26 (1997): 215–290.

43. X. Wang, D. J. Jacob, S. D. Eastham, et al., "The Role of Chlorine in Global Tropospheric Chemistry," *Atmospheric Chemistry and Physics* 19 (2019): 3981–4003.

44. C. Wang, J. Liggio, J. J. B. Wentzell, S. Jorga, A. Folkerson, and J. P. D. Abbatt, "Chloramines as an Important Photochemical Source of Chlorine Atoms in the Urban Atmosphere," *Proceedings of the National Academy of Sciences* 120 (2023): e2220889120.

45. X. Peng, T. Wang, W. Wang, et al., "Photodissociation of Particulate Nitrate as a Source of Daytime Tropospheric Cl_2," *Nature Communications* 13 (2022): 939.

46. X. Peng, W. Wang, M. Xia, et al., "An Unexpected Large Continental Source of Reactive Bromine and Chlorine With Significant Impact on Wintertime Air Quality," *National Science Review* 8 (2021): nwaa304.

47. Z. Finewax, D. Pagonis, M. S. Claflin, et al., "Quantification and Source Characterization of Volatile Organic Compounds From Exercising and

Application of Chlorine-Based Cleaning Products in a University Athletic Center," *Indoor Air* 31 (2021): 1323–1339.

48. A. Moravek, T. C. VandenBoer, Z. Finewax, et al., "Reactive Chlorine Emissions From Cleaning and Reactive Nitrogen Chemistry in an Indoor Athletic Facility," *Environmental Science & Technology* 56 (2022): 15408–15416.

49. S. D. Jorga, Y. Wang, and J. P. D. Abbatt, "Reaction of HOCl With Wood Smoke Aerosol: Impacts on Indoor Air Quality and Outdoor Reactive Chlorine," *Environmental Science & Technology* 57 (2023): 1292–1299.

50. M. M. J. W. van Herpen, Q. Li, A. Saiz-Lopez, et al., "Photocatalytic Chlorine Atom Production on Mineral Dust-Sea Spray Aerosols Over the North Atlantic," *Proceedings of the National Academy of Sciences* 120 (2023): e2303974120.

51. A. A. Angelucci, L. R. Crilley, R. Richardson, et al., "Elevated Levels of Chloramines and Chlorine Detected Near an Indoor Sports Complex," *Environmental Science: Processes & Impacts* 25 (2023): 304–313.

52. S. S. Gunthe, P. Liu, U. Panda, et al., "Enhanced Aerosol Particle Growth Sustained by High Continental Chlorine Emission in India," *Nature Geoscience* 14 (2021): 77–84.

53. J. Lelieveld, S. Gromov, A. Pozzer, and D. Taraborrelli, "Global Tropospheric Hydroxyl Distribution, Budget and Reactivity," *Atmospheric Chemistry and Physics* 16 (2016): 12477–12493.

Supporting Information

Additional supporting information can be found online in the Supporting Information section.